Improved Wind Speed Prediction Results by Artificial Neural Network Method

Asilhan Sevinc Sirdas, Akatas Nilcan, and Izgi Ercan

1 Introduction

Recently, increase in industrialization and urbanization has brought about a rise in energy demand. Orientation to renewable energy sources is inevitable because resources used in energy production have been running out, and they cause irreversible damages to the environment. Wind is one of these renewable energy resources. The most positive impact of wind energy is to not cause the release of greenhouse gases that are formed as a result of the combustion of fossil fuels. Besides, the widespread use of wind energy will also reduce pollutant emissions as a result of reduction in fossil fuel consumption (Fig. 1 and Table 1).

Turkey is under the influence of the northern wind caused by the general circulation of the atmosphere. It is also surrounded by seas on three sides and has high valleys, especially in the eastern regions. All these lead to high wind energy potential for Turkey. Turkey's gross wind potential is thought to be 400 billion kWh per year, while technical potential is thought to be 120 billion kWh per year (Gençoğlu 2002). According to the Global Wind Report published by Global Wind Energy Council, the total installed capacity of Turkey was 2312 MW at the end of 2012; then 646 MW were added in 2013, and it increased to 2959 MW at the end of 2013 (Url-1 2014).

A.S. Sirdas (✉) • A. Nilcan
Istanbul Technical University, Faculty of Aeronautics and Astronautics, Department of Meteorological Engineering, Maslak, 34469 Istanbul, Turkey
e-mail: sirdas@itu.edu.tr; ssirdas@gmail.com

I. Ercan
Yildiz Technical University, Faculty of Electrical Engineering, Davutpasa Campus, Istanbul, Turkey

F. Aloui, I. Dincer (eds.), *Exergy for A Better Environment and Improved Sustainability 2*, Green Energy and Technology,
https://doi.org/10.1007/978-3-319-62575-1_46

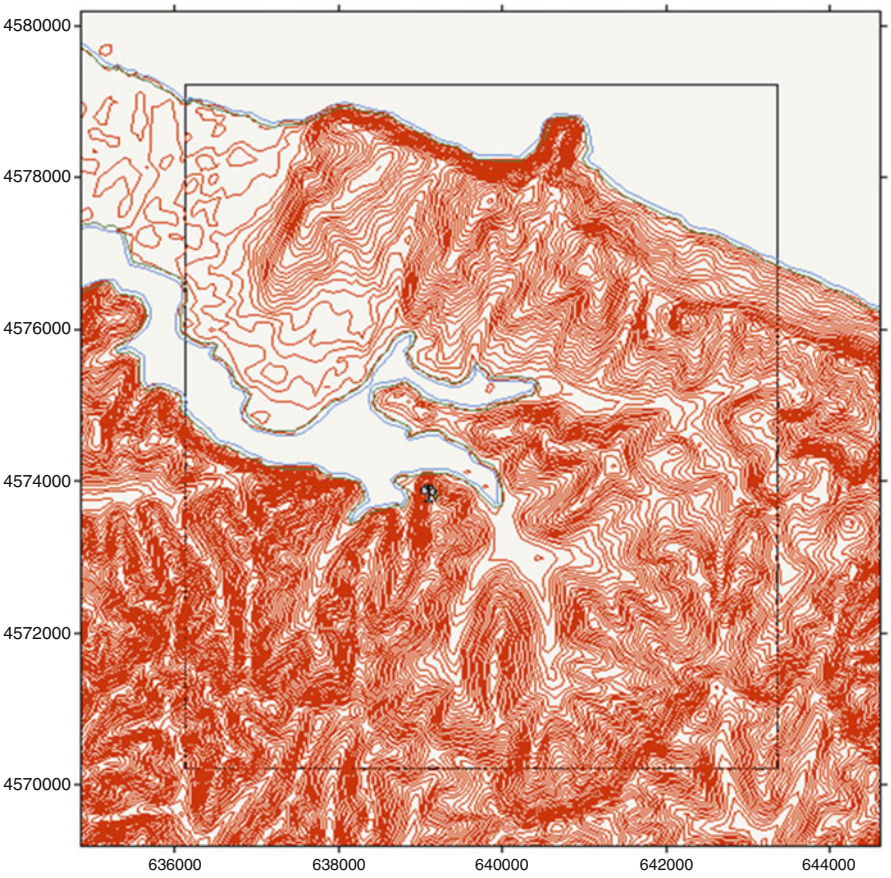

Fig. 1 Digital map of study area by WaSPV3

Turkey has continued to make new breakthroughs related to wind energy. In this respect, this work aimed to form a preliminary study for a wind turbine planned to take place in Terkos, Istanbul, as the first national turbine of Turkey. For this reason, short-term analysis and predictions of wind for Terkos region were handled in this study.

Nomenclature

V_1	The observed wind speed (m.s^{-1})
V_2	The calculated wind speed (m.s^{-1})
Z_2	The height level 2 (m)
Z_1	The height level 1 (m)
Greek letters	
α	An empirically derived coefficient that varies depending upon the stability of the atmosphere

(continued)

Superscripts	
α	0.169
Subscripts	
i	Time step
n	Number of time steps

Table 1 Roughness lengths specified in WAsP1

Physical z_0 [m]	Terrain surface characteristics	Roughness class z_0	Specified in WAsP [m]
1.5		4 (1.5 m)	1.5
>1	Tall forest		>1
1.00	City		1.00
0.80	Forest		0.80
0.50	Suburbs		0.50
0.40		3 (0.40 m)	0.40
0.30	Shelter belts		0.30
0.20	Many trees and/or bushes		0.20
0.10	Farmland with closed appearance	2 (0.10 m)	0.10
0.05	Farmland with open appearance		0.05
0.03	Farmland with very few buildings/ trees	1 (0.03 m)	0.03
0.02	Airport areas with buildings and trees		0.02
0.01	Airport runway areas		0.01
0.008	Mown grass		0.008
0.005	Bare soil (smooth)		0.005
0.001	Snow surfaces (smooth)		0.003
0.0003	Sand surfaces (smooth)		0.003
0.0002	(Used for water surfaces in the Atlas)	0 (0.0002 m)	0.0
0.0001	Water areas (lakes, fjords, open sea)		0.0

2 Data and Methodology

The study area, Terkos, is in the northwest of Istanbul, Turkey, with 41° 18′ N latitude and 28° 39′ E longitude (Fig. 2). A measurement mast with measuring instruments at 20, 40, 65, 80, and 81 m is located in the area, which is at 51 m from sea level. Temperature, pressure, wind speed, and wind direction data can be obtained on these levels at 10 min intervals. The measurement mast is shown in Fig. 3. In this study, wind speed data from August 1, 2012, to August 1, 2013, were

Fig. 2 Study area

measured at all levels. Wind direction data were obtained from 20 and 65 m of the mast for the same time period.

Due to the absence of data measured at 10 m, it was obtained from the other levels by using power law (Eq. 1):

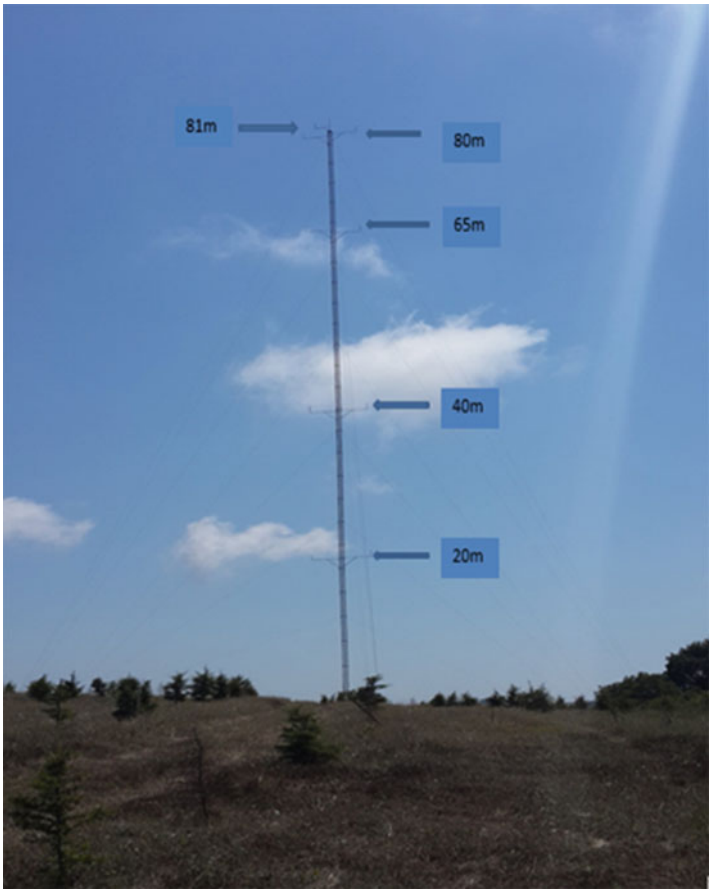

Fig. 3 Measurement mast

$$V_2 = V_1 \left(\frac{Z_2}{Z_1} \right)^{\alpha} \tag{1}$$

where V_2 (m/s) is the calculated wind speed at height z_2 (m), V_1 (m/s) is the observed wind speed at z_1 (m), and α is the power law exponent, which is affected by the roughness of the location. For the study area, α was found as 0.169.

The daily and monthly averages of wind speeds were shown by time series graphs. Daily mean wind speed time series derived from 10 min interval observation data showed that wind speeds were higher in October, November, and February (Fig. 4). Especially in the earliest days of February, wind speeds reached maximum values.

Monthly mean wind speed graphs show that wind speed values decrease in summer season of the region (May–June–July) and increase in autumn season (August–September–October) (Fig. 4). Determining the wind directions is crucial

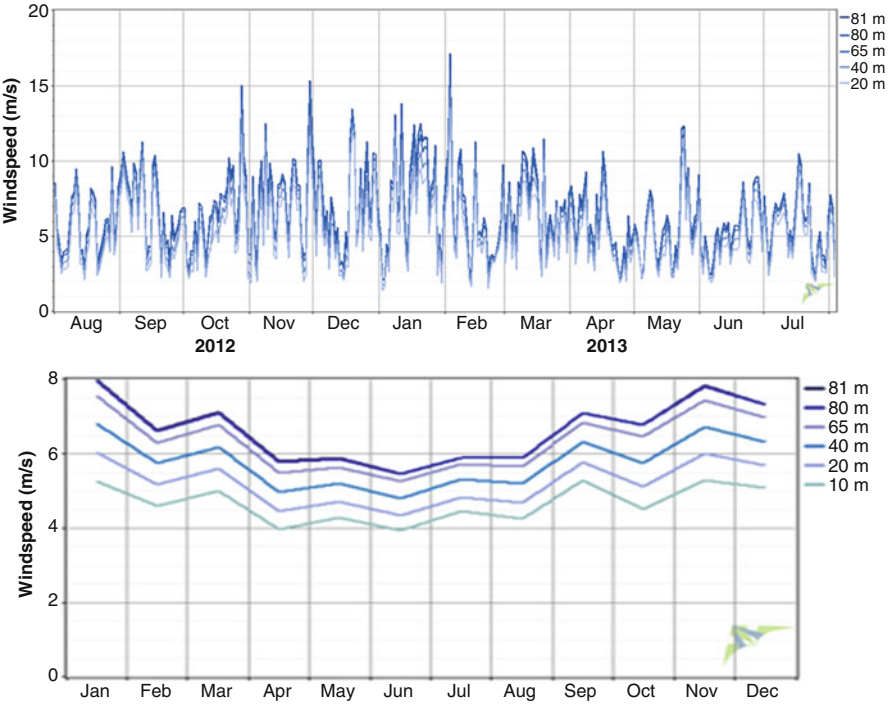

Fig. 4 Time series of daily mean wind speed

for wind energy studies. Wind roses derived from wind direction data from 20 to 65 m of measurement mast are demonstrated in Fig. 5. Accordingly, the most windward directions are northwest and southeast.

2.1 Short-Term Wind Prediction with WRF/ARW

The Weather Research and Forecasting (WRF) model has two dynamical core variants named nonhydrostatic mesoscale (NMM) and advance research (ARW). NMM is used for making operational forecasts, while ARW is used for both meteorological research and numerical weather prediction. In this study, WRF/ARW version 3.2.1 was used.

2.1.1 Initial and Boundary Conditions

The initial and boundary conditions supplied to the WRF/ARW model were provided by the National Centers for Environmental Prediction (NCEP) Final

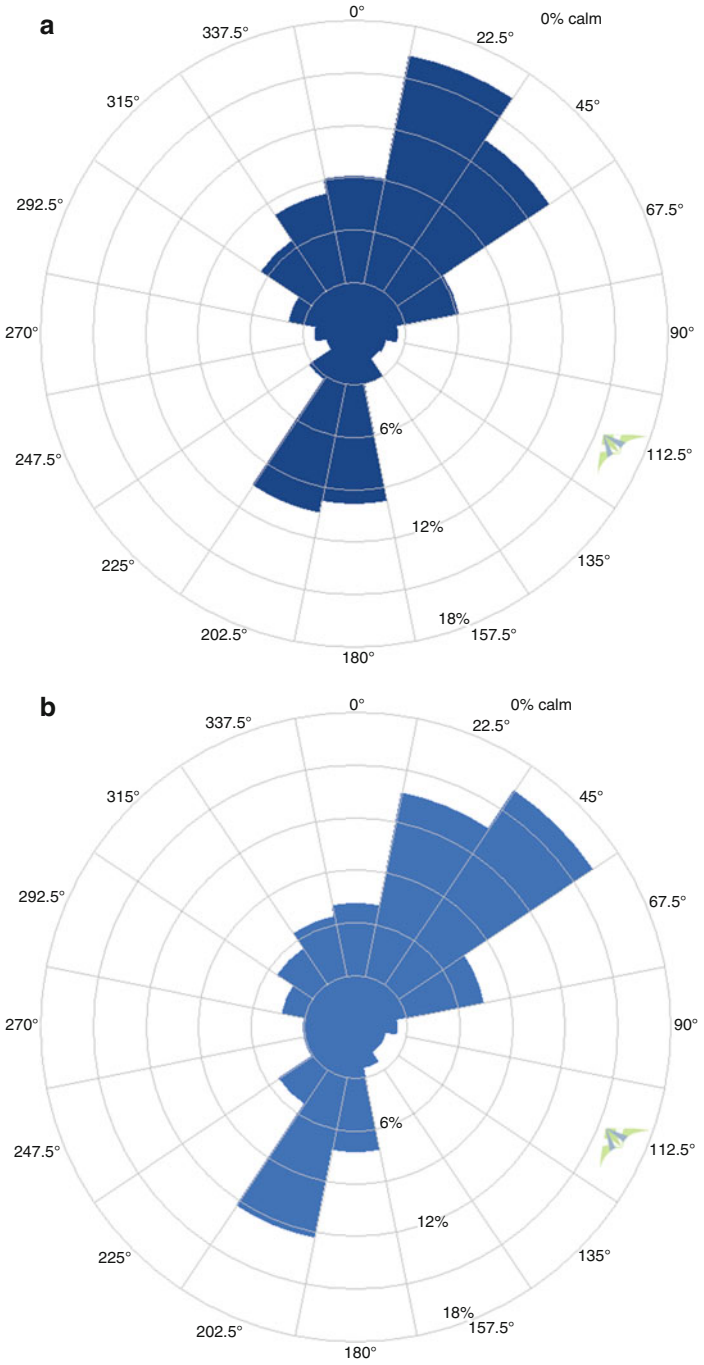

Fig. 5 Wind rose for (**a**) 65 m (**b**) 20 m

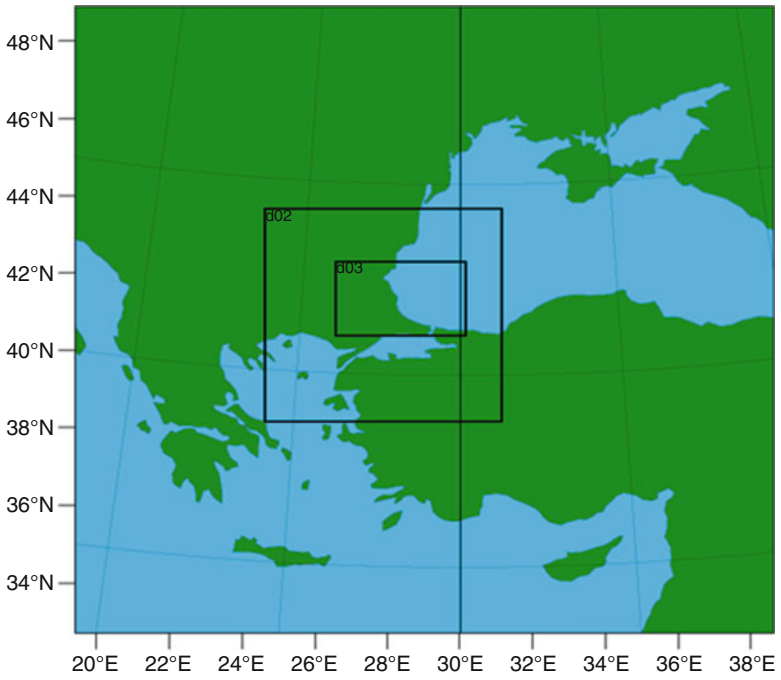

Fig. 6 WRF/ARW domain configuration

Operational Model Global Tropospheric Analyses, with 1° of spatial and 6 h of temporal resolution.

2.1.2 Design of the Simulations

The model was built over three nested domains shown in Fig. 6. The coarser domain (d01) with 30 km spatial resolution covers eastern Europe and Turkey between 33–49° N latitudes and 19–39° E longitudes. The middle domain (d02) with 10 km spatial resolution covers Marmara Region located in the northwest of Turkey. The inner domain (d03) with 3 km spatial resolution covers Thrace region and Terkos. All domains are cantered to the same point where measurement mast locates with latitude 41° 18′ N and longitude 28° 39′ E. The vertical structure of the model contains 28 layers.

There are several physical options for the WRF model predictions. These physical options consist of the combination of microphysics, cumulus parameterizations, surface physics, planetary boundary layer (PBL) physics, and atmospheric radiation physics. In this study, six different WRF/ARW simulations obtained with different physical options are listed in Table 2. It was aimed to test mainly the PBL parameterizations. In the simulations, Asymmetrical Convective Model version 2 (ACM2), Medium Range Forecast Model (MRF), Mellor–Yamada–Janjic

Table 2 WRF/ARW physics options

Parameterization	PBL	Land surface model	Surface layer physics
1	ACM2	Pleim-Xiu	Pleim-Xiu
2	MRF	Noah LSM	Monin-Obukhov
3	MYJ	Noah LSM	Eta similarity
4	MYNN2	Noah LSM	MYNN
5	YSU	Noah LSM	Monin-Obukhov
6	QNSE	Noah LSM	QNSE

Table 3 WRF/ARW PBL schemes

Scheme	WRF dynamic core	Prognostic variables	Diagnostic variables	Cloud mixing ratio
ACM2	ARW	–	–	QC, QI
MRF	ARW NMM	–	–	QC, QI
MYJ	ARW NMM	TKE_PBL	EL_PBL, exch_h	QC, QI
MYNN2	ARW	QKE	Tsq, Qsq, Cov, exch_h, exch_m	QC
YSU	ARW NMM	–	exch_h	QC, QI
QNSE	ARW NMM	TKE_PBL	EL_PBL, exch_h, exch_m	QC, QI

Url-2 (2014)

(MYJ), Mellor–Yamada Nakanishi and Niino Level 2 (MYNN2), Yonsei University (YSU), and Quasi-Normal Scale Elimination (QNSE) PBL options were used (Table 2). The differences between the PBL parameterizations are indicated in Table 3. They can differ from each other by the prognostic variables TKE_PBL (turbulent kinetic energy from PBL) and QKE (turbulent heat flux) and diagnostic variables EL_PBL (length scale from PBL), exch_h (scalar exchange coefficient), exch_m (exchange coefficient), Tsq (liquid water potential temperature variance), Qsq (liquid water variance), and Cov (liquid water-liquid water potential temperature covariance) (Url-3 2014).

According to the National Center for Atmospheric Research (NCAR) Technical Note, microphysics schemes have a wide range of options from basic physics for idealized studies to complicated mixed-phase physics for process studies and numerical weather prediction (Skamarock et al. 2008). In this study, Thompson option including both ice-phase and mixed-phase processes were chosen for all simulations as the microphysics scheme.

Another parameterization option is cumulus physics scheme. The cumulus physics schemes are responsible for the subgrid-scale effects of convective and/or shallow clouds (Skamarock et al. 2008). The Kain–Fritsch scheme including updraft and downdraft changes was used for this study. This scheme makes the calculations by using a basic cloud model bearing updrafts and downdrafts with dragging effects (Skamarock et al. 2008).

Using these parameterizations, 3-day and 10-day predictions were performed by WRF/ARW. Simulation period covered 1–4 February and 1–4 March for 3-day

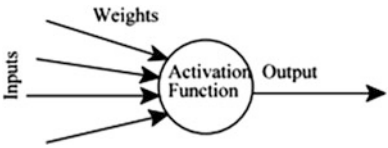

Fig. 7 An artificial neuron (Gershenson 2001)

runs. In the 10-day predictions, 1–11 February and 1–11 March periods were chosen. The results were derived as 1 h outputs.

Because the WRF/ARW gave results only for the grid points, the data on the grids were moved to Terkos where the measurement mast locates by two downscaling methods: weighted average method and nearest neighbor method.

2.2 Artificial Neural Networks (ANN)

The artificial neural network (ANN) method was used to try and reduce the errors of WRF/ARW results that were derived from different parameterizations. The ANN method is the study of cellular networks with storage of the experimental knowledge feature (Aleksander 1989). The development of ANN is known to be inspired by the neurons in the brain. The functioning of the artificial neuron is shown in Fig. 7.

An ANN model is trained using the available data and then tested with the rest of the data. The purpose of the training is to calculate the weights and minimize the errors (Aşkın et al. 2011). In this study, 70% of the WRF/ARW prediction results were used as training data and the remaining 30% data were tested.

In the ANN model, the Levenberg–Marquardt algorithm was performed. It is a least squares calculation method mainly based on the maximum neighborhood and consists of the best features of Gauss–Newton and gradient descent algorithms (Aşkın et al. 2011).

3 Applications

WRF/ARW was run with six different initial conditions, and the results were obtained. First, February 1–4 and March 1–4 results were derived. Then they were downscaled to the point where the observation data exist. Model results were achieved for the selected nesting area separately.

Hourly wind speed data (measured) were compared to the hourly model results (predicted) at 10 m. Results are shown in Figs. 8 and 9.

From a coarser domain to the inner domain, the model results were closer to the observations (Fig. 7). A bigger domain and lower resolution made predictions that

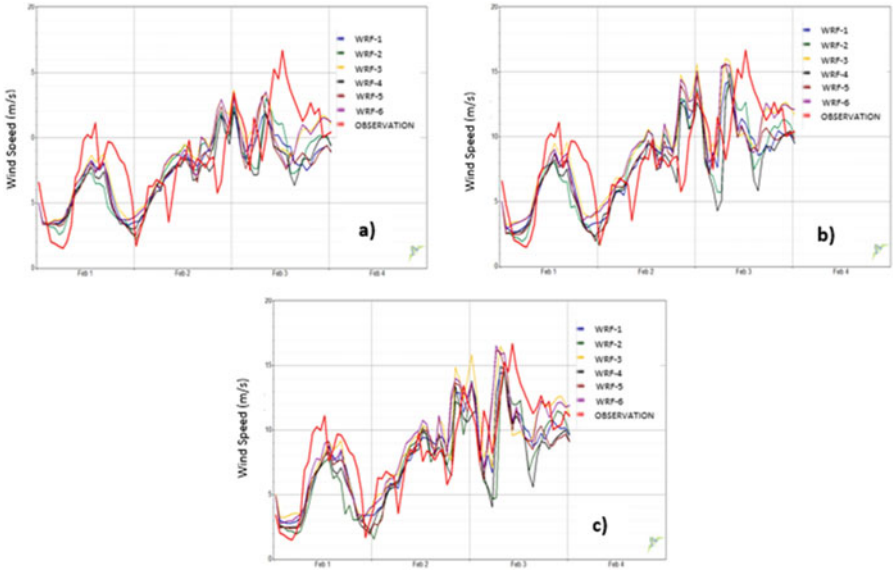

Fig. 8 1–4 February model results (downscaled by nearest neighbor method) and observations for (**a**) coarser domain (d01), (**b**) middle domain (d02), (**c**) inner domain (d03)

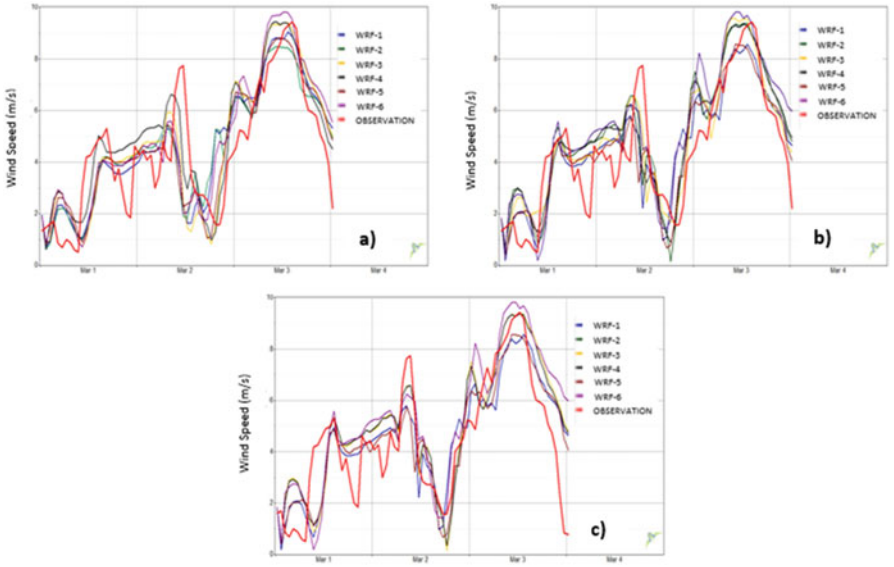

Fig. 9 March 1–4 model results (downscaled by nearest neighbor method) and observations for (**a**) coarser domain (d01), (**b**) middle domain (d02), (**c**) inner domain (d03)

were far from the observed data. The model results were seen to be close to each other, and WRF-3 results were closer to the observations.

4 Results and Discussions

4.1 WRF/ARW Predictions

Model performances were established by the root mean square error (RMSE) (Eq. 2) compared to the measured data in Terkos:

$$\mathrm{RMSE} = \sqrt{\frac{1}{n}\sum_{i=1}^{n}(F_i - O_i)} \tag{2}$$

where n is number of data, F_i is forecast values, and O_i is observed values at time i.

The RMSE calculations are given in Tables 4 and 5.

The model results belonging to March 1–4 were more successful than February 1–4 results. Where the wind speeds are high, especially in March 3, observations and predictions overlapped well (Fig. 9). Although observations had more fluctuations than the predictions, general oscillation could be followed by the simulations.

4.2 ANN Predictions

The different model predictions were used in a two-layer ANN model to get more correlated results with the observations. The first 70% of hourly March 1–11 results were inserted in the ANN as the training data. Then the remaining data were used as the test data. The predictions were attained hourly for the first 6 h. Table 6 shows the correlations and RMSE between predictions derived by using WRF/ARW simulations and observations. "1" refers to training and "2" refers to test data.

In order to make a comparison, six different WRF/ARW simulation results and ANN results using these simulations are indicated in Table 7.

Correlations between the observations and the forecasts used as the training data began to decrease at the third hour. Generated test data were more correlated to the observations when compared to the training data. Temporal variation of the correlation is noticeable in Table 5. For all WRF/ARW simulations, correlations of the first hour were very low, whereas the ANN correlations were considerably higher. The general view was that ANN increased the correlations substantially.

Table 4 RMSE results for 1–4 February

1–4 February RMSE (m/s)	WRF-1	WRF-2	WRF-3	WRF-4	WRF-5	WRF-6
D01						
Nearest neighbor	1.32	1.36	1.20	1.47	1.44	1.29
Weighted ave.	1.38	1.38	1.21	1.51	1.50	1.31
D02						
Nearest neighbor	1.16	1.17	1.09	1.20	1.17	1.12
Weighted ave.	1.35	1.38	1.20	1.44	1.39	1.27
D03						
Nearest neighbor	1.19	1.44	1.31	1.38	1.38	1.30
Weighted ave.	1.21	1.45	1.29	1.37	1.36	1.30

Table 5 RMSE results for 1–4 March

1–4 March RMSE (m/s)	WRF-1	WRF-2	WRF-3	WRF-4	WRF-5	WRF-6
D01						
Nearest neighbor	0.89	0.91	0.91	0.89	0.87	0.95
Weighted ave.	0.87	0.90	0.89	0.91	0.85	0.92
D02						
Nearest neighbor	0.70	0.71	0.80	0.86	0.70	0.87
Weighted ave.	0.78	0.89	0.84	0.86	0.70	0.83
D03						
Nearest neighbor	0.79	0.88	0.88	0.85	0.76	1.01
Weighted ave.	0.78	0.96	0.85	0.85	0.74	0.96

Table 6 ANN results

	1 h	2 h	3 h	4 h	5 h	6 h
Correlation 1	0.77	0.66	0.61	0.50	0.40	0.25
Correlation 2	0.58	0.61	0.60	0.65	0.57	0.57
RMSE 1	1.54	1.80	1.90	2.06	2.18	2.28
RMSE 2	2.23	2.17	2.34	2.29	2.46	3.05

5 Conclusions

WRF/ARW simulation results showed that inner domain results are closer to the observations than the other domains due to higher spatial resolution. In addition, the nearest neighbor downscaling method generally worked better than the weighted average method. When the wind speeds are higher than 12–13 m/s, model results were much more underestimated while comparing the rest. Because WRF/ARW is a mesoscale model, it was unable to predict the short-time variation of the winds in microscales and follow the general oscillation on time.

February results had less accuracy because of relatively high wind speed values when compared to March results. Predictions were accurate for the wind speeds less

Table 7 ANN results

	1 h	2 h	3 h	4 h	5 h	6 h
WRF-1						
Correlation	0.001	0.28	0.28	0.31	0.35	0.25
WRF-2						
Correlation	0.07	0.03	0.013	0.0008	0.22	0.44
WRF-3						
Correlation	0.013	0.17	0.19	0.25	0.21	0.17
WRF-4						
Correlation	0.016	0.18	0.24	0.28	0.25	0.23
WRF-5						
Correlation	0.046	0.011	0.001	0.034	0.039	0.06
WRF-6						
Correlation	0.02	0.27	0.29	0.35	0.34	0.22
YSA (training)						
Correlation	0.77	0.66	0.61	0.50	0.40	0.25
YSA (test)						
Correlation	0.58	0.61	0.60	0.65	0.57	0.57

than 10 m/s, especially in March results. On the contrary, the predictions were underestimated for the peak values in February.

Different parameterizations showed slightly different results. While WRF-3 and WRF-6 parameterizations had fewer errors in February predictions, WRF-1 and WRF-5 parameterizations were more successful than the others in March results.

Consequently, it was observed that different initial conditions, such as physics options or resolution, gave different results. If different scheme results are combined in ANN, much more accurate results can be obtained.

Acknowledgments This research was supported by The Scientific and Technological Research Council of Turkey (TUBITAK) 1007-KAMAG; MİLRES (National Wind Power System). We would like to acknowledge the support of TUBITAK who encouraged our research.

References

Aleksander, I.: Neural Computing Architectures: The Design of Brain-Like Machines. North Oxford Academic Publ, London (1989)

Aşkın, D., İskender, İ., Mamızadeh, A.: Farklı Yapay Sinir Ağları Yöntemlerini Kullanarak Kuru Tip Transformatör Sargısının Termal Analizi. Gazi Üniversitesi Mühendislik Mimarlık Fakültesi Dergisi Cilt. **26**(4), 9005–9913 (2011)

Gençoğlu, M.T.: Yenilenebilir Enerji Kaynaklarının Türkiye Açısından Önemi. Fırat Üniversitesi Fen ve Mühendislik Bilimleri Dergisi. **14**(2), 57–64 (2002)

Gershenson, C.: Artificial Neural Networks for Beginners, 9 pages. University of Sussex, Cognitive and computing sciences (2001)

Skamarock, W.C., Klemp, J.B., Dudhia, J., Gill, D.O., Barker, M., Duda, K.G., Huang, X.Y., Wang, W., Powers, J.G.: A description of the advanced research WRF version 3. NCAR/TN–

475+STR. National Center For Atmospheric Research Boulder Co Mesoscale and Microscale Meteorology Div (2008)
Url-1.: http://www.gwec.net/wp-content/uploads/2014/04/GWEC-Global-Wind-Report_9-April-2014.pdf . Retrieved time: 01.10.2014
Url-2.: http://www2.mmm.ucar.edu/wrf/users/docs/user_guide_V3/ARWUsersGuideV3.pdf. Retrieved time: 22.09.2014
Url-3.: http://www2.mmm.ucar.edu/wrf/users/wrfv3.5/Registry.EM_COMMON. Retrieved time: 22.09.2014